



**HAL**  
open science

# Performance Comparison of IEEE 802.11p, 802.11bd-draft and a Unique-Word-based PHY in Doubly-Dispersive Channels

Shahab Ehsanfar, Klaus Moessner, Abdul Karim Gizzini, Marwa Chafii

► **To cite this version:**

Shahab Ehsanfar, Klaus Moessner, Abdul Karim Gizzini, Marwa Chafii. Performance Comparison of IEEE 802.11p, 802.11bd-draft and a Unique-Word-based PHY in Doubly-Dispersive Channels. 2022 IEEE Wireless Communications and Networking Conference (WCNC), Apr 2022, Austin, United States. hal-03580225

**HAL Id: hal-03580225**

**<https://hal.science/hal-03580225>**

Submitted on 18 Feb 2022

**HAL** is a multi-disciplinary open access archive for the deposit and dissemination of scientific research documents, whether they are published or not. The documents may come from teaching and research institutions in France or abroad, or from public or private research centers.

L'archive ouverte pluridisciplinaire **HAL**, est destinée au dépôt et à la diffusion de documents scientifiques de niveau recherche, publiés ou non, émanant des établissements d'enseignement et de recherche français ou étrangers, des laboratoires publics ou privés.

# Performance Comparison of IEEE 802.11p, 802.11bd-draft and a Unique-Word-based PHY in Doubly-Dispersive Channels

Shahab Ehsanfar\*, Klaus Moessner\*, Abdul Karim Gizzini†, Marwa Chafii‡§

\* Professorship of Communications Engineering, Technische Universität Chemnitz, Germany

† ETIS, UMR8051, CY Cergy Paris Université, ENSEA, CNRS, France

‡ Engineering Division, New York University (NYU), Abu Dhabi 129188, UAE

§ NYU WIRELESS, NYU Tandon School of Engineering, Brooklyn, 11201, NY

{shahab.ehsan-far, klaus.moessner}@etit.tu-chemnitz.de, abdulkarim.gizzini@ensea.fr, marwa.chafii@nyu.edu

**Abstract**—In this paper, we evaluate and make a comparison of the channel estimation performance for three different frame structures of IEEE 802.11p, IEEE 802.11bd-draft and a unique-word (UW)-based physical layer (PHY). As in vehicle-to-everything communication the wireless channel conditions may vary significantly depending on the environment and vehicle velocity, severe fading in both time and frequency domains may occur. Through simulation results, we show that the UW-based PHY achieves an interference-free performance of channel estimation via a low complexity technique, whereas the 802.11bd would need to employ a high complexity approach in order to achieve a comparable estimation performance.

## I. INTRODUCTION

Vehicular communication is currently playing a major role in cellular and non-cellular wireless communication. The IEEE 802.11 amendments provide enhancements in order to facilitate advanced use cases for the non-cellular applications. The vehicle to everything (V2X) communication was initially standardized by IEEE via wireless access for vehicular environments (WAVE) and dedicated short range communication (DSRC) set of protocols. The physical layer (PHY) in DSRC is based on IEEE 802.11p, which is derived from the older WiFi generation IEEE 802.11a. In V2X communication in urban scenarios, the wireless transceiver experiences both frequency-selective- and fast-fading channel, and thus, due to small number of pilots, the IEEE 802.11p-based PHY encounters major challenges in estimating the time-varying channel. As new use cases such as cooperative driving, platooning, etc. have been introduced for the next generation V2X, the channel estimation becomes a crucial aspect in improving the reliability of the communication. Hence, the new amendment IEEE 802.11bd multiplexes frequent training signals in order to more accurately estimate and track the channel variations.

Various techniques of channel estimation has been studied for IEEE 802.11p. For instance, [1] proposed the data and pilot aided (DPA) spatial-temporal averaging (STA) approach, where the decoded data symbols are assumed as pilot subcarriers in order to estimate and track the channel variations for their consecutive symbols. The STA approach also incorporates the channel spectral and temporal correlations in order

to average and reduce the impact of noise. In addition, further classical and Bayesian approaches of the DPA scheme has been studied in [2] and references therein. Recently, different machine learning approaches based on deep neural networks (DNN) have been studied in order to improve the channel estimation performance for 802.11p [3], [4], [5], [6]. In general however, if the wireless channel is harshly doubly-dispersive, the DPA based derivations of the channel estimation become less effective, because the adjacent subcarriers and symbols tend to lose their spectral and temporal correlations, and also erroneous demapping of initial symbols causes the error to propagate through the entire transmit frame. In order to overcome the challenges of DPA-based techniques, the IEEE 802.11bd introduces frequently multiplexed midambles in the frame. In this case, the channel estimation becomes analogous to the similar single-carrier based frame designs [7]. Comparatively, unique word (UW)-based frame designs have also been shown to be promising for doubly-dispersive channels [8], [9]. In UW-based frames, the cyclic prefix (CP)—that has a random nature—has been replaced by a deterministic sequence. Hence, the UW not only provides circular channel condition for the OFDM symbol, but also allows per-symbol synchronization and channel estimation [10], [11].

In this work, we make a performance comparison of channel estimation for various frame designs, particularly, IEEE 802.11p, draft document of 802.11bd and a recently proposed UW-based PHY [9]. We will consider multiple techniques of channel estimation, i.e. a low-complexity derivation of *Bayesian* linear minimum mean squared error (LMMSE), a DNN-based approach of channel estimation as well as a sub-optimal approach based on the combination of LMMSE and *Wiener-Hopf* filtering. The comparison through numerical analysis and extensive simulations will allow us to find a trade-off between the PHY designs and their high/low complexity channel estimation techniques<sup>1</sup>.

In the following, in Sec. II, we model the transmit frames. In Sec. III, we propose multiple channel estimation techniques

<sup>1</sup>Our simulation source codes are accessible online at [12].

for different frame structures. In Sec. IV, we evaluate the performance of each approach. We conclude the paper in Sec. V.

## II. SYSTEM MODEL

### A. OFDM Modulation

Assume a sequence of  $\mathbf{b} \in \mathbb{Z}_2^{N_b}$  information bits with  $N_b$  elements to be transmitted. The raw data bits are being encoded as  $b_c \in \mathbb{Z}_2^{N_c}$ —with code-rate  $N_b/N_c$ —and consequently, the encoded data bits are being mapped into a constellation diagram, e.g.,  $2^\mu$ -QAM, resulting  $N$  complex valued data symbols  $\mathbf{d} \in \mathbb{C}^N$ . Here,  $\mu$  denotes the modulation order. Letting the subcarrier spacing  $\Delta f = 1/NT_s$  with sampling interval  $T_s$ , orthogonal frequency division multiplexing (OFDM) assumes that each subcarrier carries an element of  $\mathbf{d}$ . Thus, considering  $\mathbf{d}$  as a frequency domain data vector, the time domain data signal is obtained by taking its inverse discrete Fourier transform (IDFT), i.e.,

$$\mathbf{x}_{d,N} = \mathbf{F}^H \mathbf{d}, \quad (1)$$

where  $\mathbf{F} \in \mathbb{C}^N$  denotes the  $N$ -point DFT matrix. In order to protect the data signal from inter-symbol-interference (ISI) caused by multi-path propagation, a cyclic prefix of length  $N_{CP}$  is added to the OFDM data symbol. Formally, the CP-protected data symbol follows

$$\mathbf{x}_{d,N'} = [\mathbf{I}_N \mathbf{0}_{N-N_{CP}} \mathbf{I}_{N_{CP}}]^T \mathbf{x}_{d,N}, \quad (2)$$

where  $N' = N + N_{CP}$ .

### B. IEEE 802.11p / 11bd-draft

Consider the frame structures of Fig. 1. The long training field (LTF) in the IEEE 802.11 family consists of two known deterministic sequences used for primary synchronization and channel estimation. It is then followed by a burst of unknown data which consists of signalling as well as useful information bits. In 802.11p the LTF is used for the primary channel estimation and next, the decoded data packets are treated as pilots in order to track the variations of the channel over time<sup>2</sup>. Based on the above description, the signal transmission of 802.11p with a burst of  $B$  symbols shall be formulated as

$$\mathbf{x}_{11,p} = [\mathbf{x}_{LTF}^T \mathbf{x}_{d,N',0}^T \mathbf{x}_{d,N',1}^T \cdots \mathbf{x}_{d,N',B}^T]^T, \quad (3)$$

where  $\mathbf{x}_{LTF} \in \mathbb{C}^{N_{CP}+2N}$  denotes the column vector associated to the LTF with long CP of length  $N'_{CP}$  and two copies of a training signal (TS). In the above expression, we have omitted the *short training field* and *signaling* field as they are less relevant to the channel estimation problem.

In order to address the fast fading situations in vehicular communication, the IEEE 802.11bd-draft adds further known deterministic sequences—so called midambles—with symbol spacing  $\Delta m$  between the OFDM symbols. Thus, a full bandwidth channel estimation can be obtained at every midamble

<sup>2</sup>We also note that in 802.11p, every symbol contains four pilot tones for channel tracking. However, the pilot tones are suitable only for flat channels. Since in this work, we focus on extremely frequency selective channels, the benefit of the four pilot tones is negligible.

in order to track the fast-fading channel variations. In this case, the transmit signal follows

$$\mathbf{x}_{11,\text{bd-draft}} = [\mathbf{x}_{LTF}^T \mathbf{x}_{d,N',0}^T \mathbf{x}_{d,N',1}^T \mathbf{x}_{d,N',2}^T \mathbf{x}_{MID} \mathbf{x}_{d,N',3}^T \cdots]^T, \quad (4)$$

where  $\mathbf{x}_{MID} \in \mathbb{C}^{N'}$  denotes the training signal associated to the midambles. In the particular case of (4), we have set  $\Delta m = 4$  as an example of the 802.11bd-draft frame format, although in general, this parameter should be accurately chosen according to the channel mobility conditions.

### C. Unique-Word-based Frames

UW sequences are deterministic sequences known to the receiver that are not only used as observations for the channel estimation, but also they provide circular channel conditions for the data packets. Fig. 1 shows an example of how UW-based data symbols are being compared to CP-based symbols. In CP-based symbols, the data symbols are ISI-free and they experience circular convolution with the wireless channel. However, the CP part—that is a random sequence—is being discarded at the receiver. In UW-based symbols, the same goals of having ISI-free symbols as well as circular convolution of the data part with the wireless channel is achieved, and additionally, since the UW sequences are deterministic and known to the receiver, they can be exploited for synchronization and channel estimation. In this regard, the UW-based symbol is defined as

$$\mathbf{x}_{UW\text{-symp}} \triangleq [\mathbf{x}_{UW}^T \mathbf{x}_{d,N}^T]^T. \quad (5)$$

Considering a burst type of communication similar to the IEEE 802.11p/bd, the UW-based frame is formulated as

$$\mathbf{x}_{UW\text{-frame}} = [\mathbf{x}_{LTF}^T \mathbf{x}_{UW\text{-symp},1}^T \mathbf{x}_{UW\text{-symp},2}^T \cdots \mathbf{x}_{UW\text{-symp},B}^T \mathbf{x}_{UW}^T]^T, \quad (6)$$

where  $\mathbf{x}_{UW} \in \mathbb{C}^{N_{CP}+N_{UW}}$  denotes the UW sequence. In this particular case, the UW sequence has length  $N_{CP} + N_{UW}$ , in which the CP part is subject to ISI from the previous data symbol and the second part is ISI-free. Notice that the data symbol does not include a CP and via *cyclic signal reconstruction* at the receiver, the FFT size can be set to the CP-less OFDM data symbol (see the proof in [9]).

### D. Wireless Channel

Transmitting the signal  $\mathbf{x}_{\text{tot}} \in \{\mathbf{x}_{11,p}, \mathbf{x}_{11,\text{bd-draft}}, \mathbf{x}_{UW\text{-frame}}\}$  over a time-varying frequency-selective channel yields

$$\mathbf{y}_{\text{tot}} = \mathbf{H}_{\text{lin}} \mathbf{x}_{\text{tot}} + \mathbf{w}_{\text{tot}}, \quad (7)$$

where  $\mathbf{H}_{\text{lin}}$  denotes matrix associated to the linear convolution of transmit signal with the instantaneous channel impulse responses (CIR), and  $\mathbf{w}_{\text{tot}}$  denotes the additive white Gaussian noise (AWGN) process. Assuming that the transmit signals satisfy the CP conditions and the observations are periodical signals with circular channels, we extract the frequency domain observations by taking the DFT over the periodical parts of the time domain training symbols. Thus,

$$\tilde{\mathbf{y}} = \tilde{\mathbf{H}} \tilde{\mathbf{x}} + \tilde{\mathbf{w}} \quad (8)$$

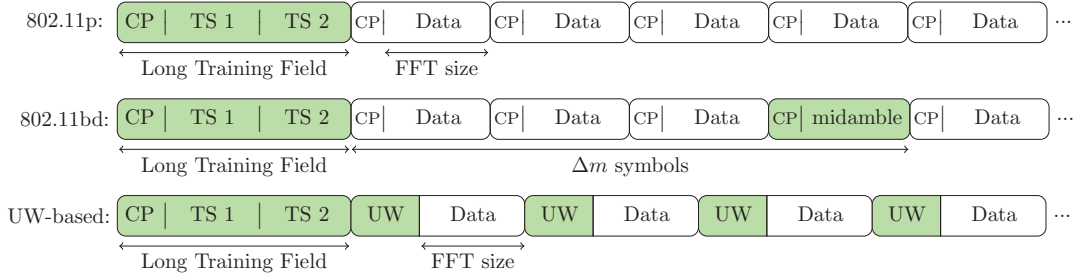


Fig. 1. Frames structures for the two IEEE 802.11p/bd technologies and the UW-based approach. Depending on the channel conditions, the UW sequences may or may not embed their own CP. The LTF for the UW-based symbols is also optional as it eases larger carrier frequency offset estimations [10].

where  $\tilde{\mathbf{x}} = \mathbf{F}\mathbf{x}$  and  $\tilde{\mathbf{y}} = \mathbf{F}\mathbf{y}$ , and  $\mathbf{y} \in \{\mathbf{y}'_{\text{LTF}}, \mathbf{y}'_{\text{MID}}, \mathbf{y}'_{\text{UW}}\}$  would be associated to  $\mathbf{x} \in \{\mathbf{x}'_{\text{LTF}}, \mathbf{x}'_{\text{MID}}, \mathbf{x}'_{\text{UW}}\}$ , respectively. Here,  $\mathbf{x}'_{\text{LTF}}$  has been obtained by removing the CP and averaging the two symbols of  $\mathbf{x}_{\text{LTF}}$ . Similarly,  $\mathbf{x}'_{\text{MID}}$  and  $\mathbf{x}'_{\text{UW}}$  are associated to the CP-less parts of  $\mathbf{x}_{\text{MID}}$  and  $\mathbf{x}_{\text{UW}}$ , respectively<sup>3</sup>. Thanks to the CP, the frequency domain channel matrix  $\hat{\mathbf{H}}$  is diagonal and it holds the channel frequency response (CFR) on its diagonal terms. In (8),  $\tilde{\mathbf{w}}$  denotes the frequency counterpart of the AWGN process.

### III. CHANNEL ESTIMATION

#### A. Primary Estimation

Based on the receiver knowledge of the preamble sequence in IEEE 802.11p, and additionally, the knowledge of midambles—in IEEE 802.11bd-draft—and unique words—in UW-frame—an initial data-aided channel estimation is carried out. The OFDM channel estimation techniques are generally derived from either *classical* least squares (LS) estimation or the *Bayesian* LMMSE estimation. The LS estimation has the advantage of lower complexity with respect to the LMMSE estimation, whereas the Bayesian LMMSE exploits *a-priori* knowledge of the channel statistics in order to achieve higher performance, at the cost of higher complexity. Considering the channel estimation procedures in frequency domain, the two LS and LMMSE estimations are given by

$$\hat{\mathbf{h}}'_{\text{LS}} = (\mathbf{X}^H \mathbf{X})^{-1} \mathbf{X} \tilde{\mathbf{y}}, \quad (9)$$

$$\hat{\mathbf{h}}'_{\text{LMMSE}} = \mathbf{R}_{hh} \mathbf{X}^H (\mathbf{X} \mathbf{R}_{hh} \mathbf{X}^H + \sigma^2 \mathbf{I}_N)^{-1} \tilde{\mathbf{y}}, \quad (10)$$

respectively. Here,  $\mathbf{R}_{hh} = \mathbb{E}[\tilde{\mathbf{h}}\tilde{\mathbf{h}}^H]$  denotes the frequency domain channel auto-correlation matrix, and  $\sigma^2$  denotes the noise variance. Note that  $\mathbf{X} = \text{diag}(\tilde{\mathbf{x}})$  is a diagonal matrix and thus, low complexity subcarrier-wise estimation of the elements of  $\hat{\mathbf{h}}'_{\text{LS}}$  is achieved by  $\hat{h}'_{\text{LS}}[k] = \tilde{y}[k]/\tilde{x}[k]$ .

We also consider a low-complexity frequency domain approximation of LMMSE (ALMMSE) channel estimation where the *a-priori* knowledge of the channel characteristics is being neglected, and thus, the channel auto-correlation matrix  $\mathbf{R}_{hh}$  is set to identity matrix. We assume, however,

<sup>3</sup>In order to have an ISI-free observation of the UW sequence, we additionally assume that the UW sequences include a CP part in them.

that the noise variance is available. Hence, the low-complexity ALMMSE yields

$$\hat{h}'[k] = \frac{\tilde{x}[k]^*}{\tilde{x}[k]^* \tilde{x}[k] + \sigma^2}. \quad (11)$$

Assuming that the knowledge of the number of CIR taps  $L$  is available at the receiver, we apply a discrete Fourier transform (DFT)-based filtering to the estimation  $\hat{\mathbf{h}}'$ . Analogously to the approach in [13], the filtering is accomplished by multiplying the IDFT of the estimation by an  $L$ -length rectangular window, or simply, taking the first  $L$  taps of the estimated CIR, i.e.,

$$\hat{\mathbf{h}} = (\mathbf{F}^H \hat{\mathbf{h}}')_{1:L}. \quad (12)$$

As an alternative reference, we also consider frequency domain smoothing of the CFR estimation by a filter  $\mathbf{g}$  that spans over  $K$  subcarriers, i.e.,

$$\hat{\mathbf{h}}_{\mathbf{g}} = \hat{\mathbf{h}}' * \mathbf{g}. \quad (13)$$

#### B. Time domain Wiener filtering

We consider the *Wiener-Hopf* filter as a sub-optimal statistical approach on smoothing the channel estimations on reference symbols—i.e. midambles of 11.bd-draft and UW of UW-frame—and also predicting the channel for the data symbols. Thus, assuming  $s < B$  reference symbols—either as midamble or UW—are transmitted, the Wiener-Hopf filter analogously as in [9] averages the time domain estimations and also interpolates them for the data symbols. In this case, including the preamble,  $s + 1$  channel impulse responses

$$\hat{\mathbf{H}} = [\hat{\mathbf{h}}_0 \ \hat{\mathbf{h}}_1 \ \dots \ \hat{\mathbf{h}}_s] \quad (14)$$

are available to be filtered. Here,  $\hat{\mathbf{h}}_s \in \mathbb{C}^{N_{\text{CP}}}$  is the result of IDFT operation on  $\hat{\mathbf{h}}_{\text{FD}}$  and truncating it to  $N_{\text{CP}}$  samples. The filtered CIR's  $\ell$ -th tap at reference symbol  $s$  is given by

$$h_s[\ell] = \mathbf{R}_d^H (\mathbf{R}_{\text{ref}} + \hat{\sigma}^2 \mathbf{I}_{(b+1)})^{-1} \hat{\mathbf{h}}_\ell, \quad (15)$$

where  $\hat{\mathbf{h}}_\ell$  denotes the  $\ell$ -th row of  $\hat{\mathbf{H}}$  and  $\hat{\sigma}^2$  denotes the variance of CIR estimation at tap  $\ell$ . Furthermore,

$$[\mathbf{R}_d]_{m,n} = \mathbb{E}[h_\ell[m]^* h_\ell[n]] \text{ for } n \in \mathcal{S} \text{ and } m \in \mathcal{D} \quad (15a)$$

where  $\mathcal{S}$  denotes the set of indexes associated to the reference symbols, and  $\mathcal{D}$  is associated to the data symbols for which the channel needs to be predicted. Additionally,

$$[\mathbf{R}_{\text{ref}}]_{n,n} = \mathbb{E}[h_\ell[n]^* h_\ell[n]] \text{ for } n \in \mathcal{S}. \quad (15b)$$

Since the channel modeling in (7) does not include any non-linear mapping, we expect (15) to provide the optimal performance and a lower bound in terms of estimation error. Nevertheless, the above Wiener filtering approach requires *a-priori* knowledge of the channel distribution both in terms of spatial and temporal correlations.

### C. deep neural network

In order to further improve the low-complexity ALMMSE channel estimation of (11) and (13), we consider a DNN approach in which the channel statistics are learnt by the network through the concept of *learning from examples* or *supervised learning*. The data set consists of a training set  $[\mathbf{i}, \mathbf{t}]$  where  $\mathbf{i}$  denotes a measurement vector and  $\mathbf{t}$  a target vector [14]. We consider the DNN-based channel estimation in three main stages:

i) *Data set arrangement*: Whether for training or testing, a proper arrangement of the input data in form of the vector  $\mathbf{i}_{(0)}$  is necessary. In [3] and [4], the estimated frequency domain channel coefficients were used as the input vector, where [3] considered the initial LS channel estimation and [4] considered an extra stage of spatial-temporal averaging. Similarly, we let the frequency domain estimation  $\mathbf{i}_{\text{FD},(0)} \leftarrow \hat{\mathbf{h}}$  be the DNN measurement vector and the true frequency response  $\mathbf{t}_{\text{FD}} \leftarrow \mathbf{h}$  be the target vector.

ii) *DNN architecture and training*: Consider a  $Q$ -layer DNN with one input layer, one output layer, and  $Q - 2$  hidden layers. Each hidden layer consists of  $1 \leq j \leq J$  neurons, where  $J$  is the maximum number of neurons in a single hidden layer. Each neuron  $j$  at layer  $q$  calculates a non-linear function

$$o_{(q,j)} = f_{(q,j)}(\mathbf{w}_{(q,j)}^T \mathbf{i}_{(q)} + b_{(q,j)}) \quad (16)$$

over its input vector  $\mathbf{i}_{(q)}$ . The weight vector  $\mathbf{w}_{(q,j)}$  and the bias term  $b_{(q,j)}$  are learnable parameters. The function  $f(\cdot)$  denotes a non-linear activation function. Stacking the outputs of the neurons of a single layer  $q$  in form of vector  $\mathbf{o}_{(q)}$  and setting it as the input of the next layer  $\mathbf{i}_{(q+1)} \leftarrow \mathbf{o}_{(q)}$  yields

$$\mathbf{i}_{(q+1)} = \mathbf{f}_{(q)}(\mathbf{W}_{(q)}^T \mathbf{i}_{(q)} + \mathbf{b}_{(q)}). \quad (17)$$

The weight matrix  $\mathbf{W} \supseteq \mathbf{W}_{(q)}$  and the bias matrix  $\mathbf{B} \supseteq \mathbf{b}_{(q)}$  over all hidden layers has to be chosen such that the cost function  $C(\mathbf{o}, \mathbf{t})$  is minimized, i.e.

$$[\mathbf{W}, \mathbf{B}] = \arg \min_{\mathbf{W}, \mathbf{B}} C(\mathbf{o}, \mathbf{t}). \quad (18)$$

In this work, we consider the channel estimation mean squared error (MSE) as the cost function, i.e.

$$C(\mathbf{o}, \mathbf{t}) = \frac{1}{N} \sum_n^N |\hat{\mathbf{h}}_{\text{FD}}[n] - \tilde{\mathbf{h}}[n]|^2. \quad (19)$$

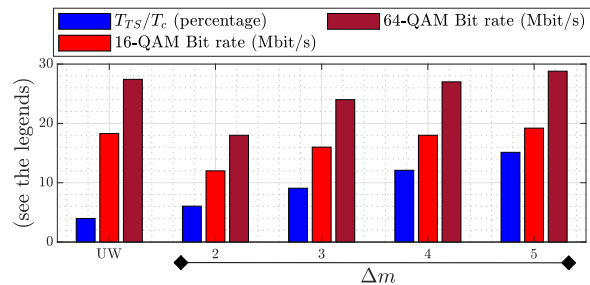


Fig. 2. Peak Data-rate vs. Channel Selectivity ratio  $\frac{T_{RS}}{T_c}$ . Due to the ISI caused by the Doppler effect, the peak data-rate might not be achievable if  $\frac{T_{RS}}{T_c}$  is large. Increase of  $\frac{T_{RS}}{T_c}$  yields the channel to vary more quickly and thus, the channel estimation error floor to limit the data-rate performance.

During the training phase, both vectors  $\mathbf{i}_{(0)}$  and  $\mathbf{t}$  are assumed to be known to the system. Moreover, the optimization algorithms for minimizing  $C(\mathbf{o}, \mathbf{t})$  are generally based on gradient descent approaches [14], [15].

iii) *Results Post-processing*: Once the DNN has been trained, we use a new set of channel realizations derived from the same model or the same dataset measured from the same environment in order to evaluate the performance of the trained DNN. At this stage,  $\mathbf{t}$  is only known to the evaluation system, without a feedback to the DNN recognition part.

## IV. NUMERICAL ANALYSIS AND SIMULATION RESULTS

In this section, we evaluate the performance of the proposed algorithms with respect to the state-of-the-art approaches via Monte Carlo simulations. Analogous to WiFi devices, the carrier- and the sampling frequencies are set to  $f_c = 5.9$  GHz and  $f_s = 10$  MHz, respectively. We consider a doubly-dispersive channel in which the multipath rays belong to a Rayleigh distribution. The power-delay-profile with maximum delay spread of 800ns is exponentially decaying from 0 to -20 dB. The users are assumed to be moving with high relative velocity of around 300 kph, being influenced by maximum Doppler shift of 1600 Hz. Each tap of the CIR is assumed to be temporally correlated according to [16]  $\ell_{n,n'} = J_0(2\pi(n - n')f_D T_s)$ , where  $J_0(\cdot)$  denotes the zeroth order Bessel function of the first kind and  $T_s$  denotes the symbol interval. The DNN hyperparameters are selected analogously as in [4], i.e. 3 hidden layers with ReLU activation function, ADAM optimizer, 500 epochs, batch size of 128 and learning rate 0.001. The number of neurons inside each layer has been chosen empirically in form of 35-18-35.

We initiate the numerical analysis by comparing the peak data-rate of the 802.11bd-draft as well as UW-based PHY with respect to channel selectivity. In this comparison the UW/midamble as well as CP overhead has been calculated analogously as in [9]. Fig. 2 depicts the peak data-rate of the two frame structures for two example modulation schemes of 16-QAM and 64-QAM. The peak data-rate only shows the bit-rate achievable by the available number of data resources. Along with the peak data-rate illustrations, the channel selec-

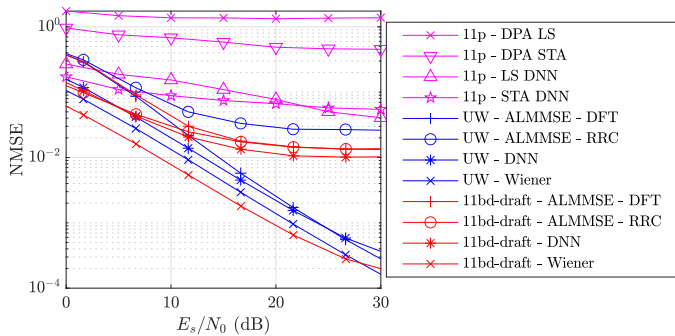


Fig. 3. Channel Estimation Performance. The Wiener filtering approaches have the highest complexity.

tivity ratio  $T_{TS}/T_c$  has also been shown as blue bars. Here,  $T_{TS}$  denotes the training symbol interval, and  $T_c$  denotes the coherence time. For an interference-free communication in time-varying scenario  $T_c \gg T_{TS}$  must hold. In Fig. 2, the first group of bars (left) is associated to the UW-based frame design, the next four groups are associated to the .11bd-draft with different midamble spacing  $\Delta m$ . According to Fig. 2, it is apparent that in .11bd-draft frame structure, by reducing  $\Delta m$  from 5 to 2—in order to achieve smaller  $T_{TS}/T_c$  ratio—also the peak data-rate reduces. On the contrary, the UW-based frame design, achieves the smallest  $T_{TS}/T_c$  ratio, which makes it more likely to combat the channel estimation error floor caused by the Doppler effect.

The channel estimation results in terms of MSE have been provided in Fig. 3. Here, all the frame formats of 802.11p, 802.11bd-draft and UW have the same preamble structure and afterwards, a burst of 120 data symbols are being transmitted. After the preamble, the .11p frame format transmits only data symbols. Since the channel varies over time, the decoded symbols are being treated as virtual pilots in order to re-estimate the channel for their consecutive symbols. Clearly, if decoding the early arrived symbols is erroneous, an erroneous channel estimation would propagate through the entire frame of 120 symbols, causing large error floors in both DPA estimation schemes of LS and STA. On the other hand, one may observe that for such a doubly-dispersive channel, applying DNN to the LS and STA approaches of the 802.11p improves their performance by approximately one order of magnitude. Nevertheless, the two DNN approaches still suffer from large error floors which is indeed due to the error propagation when attempting to update the channel estimations via prior decoded data symbols. In the IEEE 802.11bd-draft frame format, a midamble has been embedded in the frame with  $\Delta m = 4$ . In this case, for the transmission of 120 data symbols, 40 midambles are utilized. Therefore, in order to deliver the same amount of information as in 802.11p, a total number of 160 symbols must be transmitted, resulting in reduction of the data-rate. In Fig. 3 the ALMMSE-based channel estimation techniques for the 802.11bd-draft consist of two different frequency domain averaging, i.e. DFT-based filtering via (12) and frequency domain smoothing via (13).

Here, the DFT-based filtering takes the first  $L = 8$  taps, whereas the frequency domain smoothing approach uses root-raised-cosine (RRC) filter  $g$  with roll-off factor  $\beta = 0.5$  and spanned over 3 subcarriers. Additionally, in order to estimate the channel at data symbols, two approaches of piecewise-constant interpolation as well as Wiener-Hopf filter are being applied to the midamble-based channel estimations. In Fig. 3, it is clear that the channel estimation performance has significantly improved with respect to the .11p frame structure. Comparing the performance of RRC and DFT based filtering, we observe that at low SNR values, the RRC filter outperforms the DFT-based filtering, albeit, both approaches reach to the same level of error floor due to the interference terms at high SNR values. Applying DNN to the DFT-based filtering, nearly 5dB gain is achieved for low SNR values. In case of UW-based frame structure, we consider an orthogonal polyphase UW sequence [9] with  $N_{CP} = 16$  and for the sake of a reasonable UW per symbol overhead  $N_{UW} = 25$ . The ALMMSE-based channel estimation schemes are applied to the UW sequences surrounding each symbol and then averaged by two, in order to obtain an estimate at the center of the data symbol. As can be seen in Fig 3, there exists a large gap of performance between the two ALMMSE-based channel estimation schemes of DFT-based vs. RRC-based filtering. Keeping in mind that the DFT size for the channel estimation in UW-based frames is  $N_{UW}$ , the same bandwidth of 10MHz would be observed by 25 subcarriers, which is different from 64 subcarrier observations of .11bd-draft midambles. Henceforth, the .11bd-draft would have a higher resolution in capturing the channel selectivity in frequency domain, whereas, the 25 subcarriers in UW sequences are spread over a broader range of frequencies. Under such circumstances, the RRC filtering even though with 3 subcarriers-averaging causes to lose a significant amount of channel selectivity information, leading to a large error floor. On the other hand, the DFT-based filtering, accurately captures the channel selectivity information, resulting no error floor at high SNR regions. The above estimation techniques are also compared with the sub-optimal Wiener-Hopf filtering for the two frame structures of UW sequences and .11bd-draft. The Wiener filtering approach uses the individual estimations at the UW/midamble and predicts the channel at the center of the data symbols. Notably in Fig. 3, the Wiener filter diminishes the error floor at high SNR regions for the .11bd frames, which is mainly due to the more accurate time-domain prediction than the piecewise-constant interpolation. We also observe that, from the MSE optimality perspective provided by the Wiener filters, the .11bd frame structure outperforms the UW-based frame structures because of the higher power embedded in the midamble sequences, i.e., constant energy  $N = 64$  samples vs.  $N_{UW} = 25$  samples. Nonetheless in this scenario, calculation of the Wiener-filter coefficients requires *a-priori* knowledge of spectral and temporal channel statistics, which in practice requires extensive channel sounding and measurements for highly mobile vehicles/devices. Additionally, the complexity growth of the different estimation techniques are summarized in Table. I.

TABLE I  
COMPLEXITY GROWTH OF THE ESTIMATION TECHNIQUES

LS, STA	$\mathcal{O}(N^2)$
ALMMSE-RRC	$\mathcal{O}(KN^2)$
ALMMSE-DFT	$\mathcal{O}(N^2) + \mathcal{O}(N \log_2 N)$
ALMMSE-DFT-DNN	$\mathcal{O}(N^2) + \mathcal{O}(N \log_2 N) + \mathcal{O}(QN^2)$
ALMMSE + Wiener filter	$\mathcal{O}(N^2) + \mathcal{O}(B^3/\Delta m^3)$

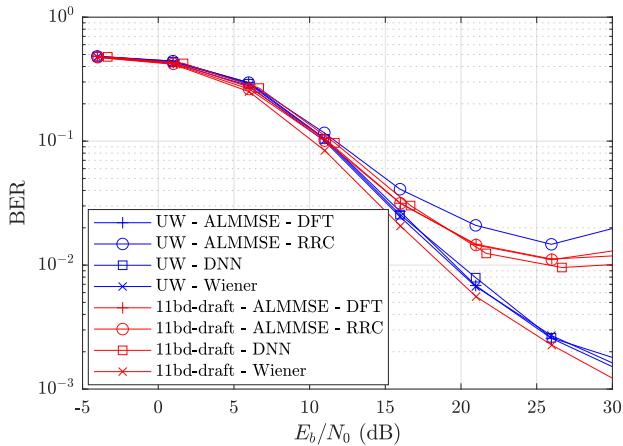


Fig. 4. Bit Error Rate Performance. For .11bd-draft, employment of Wiener filter is necessary in order to suppress the error floor. The UW-ALMMSE-DFT achieves a similar performance with low complexity.

The simulation of the bit error rate (BER) results has been provided in Fig. 4. As the channel estimation MSE results exhibit lack of sufficient performance for .11p frame format, we only compare the results for UW-based frames vs. the .11bd-draft frames. Here, the information bits are encoded via parallel concatenated convolutional codes with code rate  $r = 1/3$  and generator polynomial (133,171). The encoded and interleaved bits are mapped to 16-QAM constellation diagram before being modulated by OFDM. Moreover, in case of the UW-based frames, the receiver applies circular channel reconstruction according to [9]. Following in line with the MSE results, it can be seen that the only error-floor-free BER for the 802.11bd-draft frame format is the sub-optimal Wiener-Hopf filter. The harsh channel variations caused by the large Doppler effect yield the performance of .11bd-draft whether with DFT filtering, RRC filtering, or DNN, to be limited to around 1%, that is to say, employment of the Wiener-filter for .11bd-draft frames becomes inevitable. On the other hand, the UW-based frame structure with ALMMSE-based channel estimation and DFT-based filtering achieves a performance significantly close to both DNN as well as the Wiener-filtered approach. Unsurprisingly, the Wiener-filtering does not provide significant improvement to the BER performance of UW - ALMMSE - DFT scheme because the modulation and coding gain dominates the small 2.8 dB MSE gain of the Wiener filter.

## V. CONCLUSION

In summary, this paper addresses the channel estimation for V2X communication via various classical, Bayesian, and dNN approaches. The simulation results show that large training symbol intervals in IEEE 802.11bd-draft document cause the low complexity channel estimation schemes to suffer from large error floors and thus, unable to achieve low target BER values. On the other hand, we observe that the proposed UW-based frame design with low complexity approach of channel estimation achieves a similar performance as in high complexity channel estimation approach of the 802.11bd-draft.

## ACKNOWLEDGMENT

This work was partly supported by the European Union's Horizon 2020 research and innovation program DEDICAT 6G project under grant agreement No. 101016499.

## REFERENCES

- [1] J. A. Fernandez, K. Borries, L. Cheng, B. V. Kumar, D. D. Stancil, and F. Bai, "Performance of the 802.11p Physical Layer in Vehicle-to-Vehicle Environments," *IEEE Trans. on Veh. Technol.*, pp. 3–14, 2011.
- [2] J.-Y. Choi, C. Mun, and J.-G. Yook, "Adaptive Channel Estimation Based on a Decision Method Using a Long Preamble for the IEEE 802.11p," in *2017 IEEE 85th Vehicular Technology Conference (VTC Spring)*. IEEE, 2017, pp. 1–5.
- [3] S. Han, Y. Oh, and C. Song, "A Deep Learning Based Channel Estimation Scheme for IEEE 802.11p Systems," in *IEEE International Conference on Communications (ICC)*. IEEE, 2019, pp. 1–6.
- [4] A. K. Gizzini, M. Chafii, A. Nimr, and G. Fettweis, "Deep Learning Based Channel Estimation Schemes for IEEE 802.11p Standard," *IEEE Access*, vol. 8, pp. 113 751–113 765, 2020.
- [5] A. K. Gizzini, M. Chafii, S. Ehsanfar, and R. M. Shubair, "Temporal Averaging LSTM-based Channel Estimation Scheme for IEEE 802.11p Standard," in *Proc. of the IEEE Global Communications Conference (GLOBECOM'21)*, 2021.
- [6] A. K. Gizzini, M. Chafii, A. Nimr, R. M. Shubair, and G. Fettweis, "CNN Aided Weighted Interpolation for Channel Estimation in Vehicular Communications," *IEEE Transactions on Vehicular Technology*, vol. 70, no. 12, pp. 12 796–12 811, 2021.
- [7] Y. R. Zheng and C. Xiao, "Channel Estimation for Frequency-Domain Equalization of Single-Carrier Broadband Wireless Communications," *IEEE Trans. on Vehicular Technology*, vol. 58, no. 2, pp. 815–823, 2008.
- [8] M. Huemer, A. Onic, and C. Hofbauer, "Classical and Bayesian Linear Data Estimators for Unique Word OFDM," *IEEE Trans. on Signal Process.*, vol. 59, no. 12, pp. 6073–6085, 2011.
- [9] S. Ehsanfar, M. Chafii, and G. P. Fettweis, "On UW-Based Transmission for MIMO Multi-Carriers With Spatial Multiplexing," *IEEE Trans. on Wireless Communications*, vol. 19, no. 9, pp. 5875–5890, 2020.
- [10] S. Ehsanfar, M. Chafii, and G. Fettweis, "A Study on Unique-Word based Synchronization for MIMO Systems over Time-Varying Channels," in *2020 IEEE Wireless Communications and Networking Conference (WCNC)*. IEEE, 2020, pp. 1–7.
- [11] C. Hofbauer, W. Haselmayr, H.-P. Bernhard, and M. Huemer, "On the Inclusion and Utilization of Pilot Tones in Unique Word OFDM," *IEEE Trans. on Signal Process.*, vol. 68, pp. 5504–5518, 2020.
- [12] S. Ehsanfar. (2022) Channel Estimation 802.11p 802.11bd UW-PHY. [Online]. Available: <https://github.com/shahab-ehsanfar/Channel-Estimation-UW-802-11p-11bd>
- [13] S. Ehsanfar, M. Matthé, D. Zhang, and G. Fettweis, "Theoretical Analysis and CRLB Evaluation for Pilot-aided Channel Estimation in GFDM," in *Proc. of the IEEE Global Communications Conference (GLOBECOM'16)*, 2016.
- [14] J. Schürmann, *Pattern Classification: A Unified View of Statistical and Neural Approaches*. Wiley, 1996.
- [15] S. De, A. Mukherjee, and E. Ullah, "Convergence guarantees for RMSProp and ADAM in non-convex optimization and an empirical comparison to Nesterov acceleration," *arXiv preprint:1807.06766*, 2018.
- [16] R. H. Clarke, "A Statistical Theory of Mobile-Radio Reception," *Bell system technical journal*, vol. 47, no. 6, pp. 957–1000, 1968.